Article

Structure

The Ribosomal Protein uL22 Modulates the Shape of the Protein Exit Tunnel

Graphical Abstract

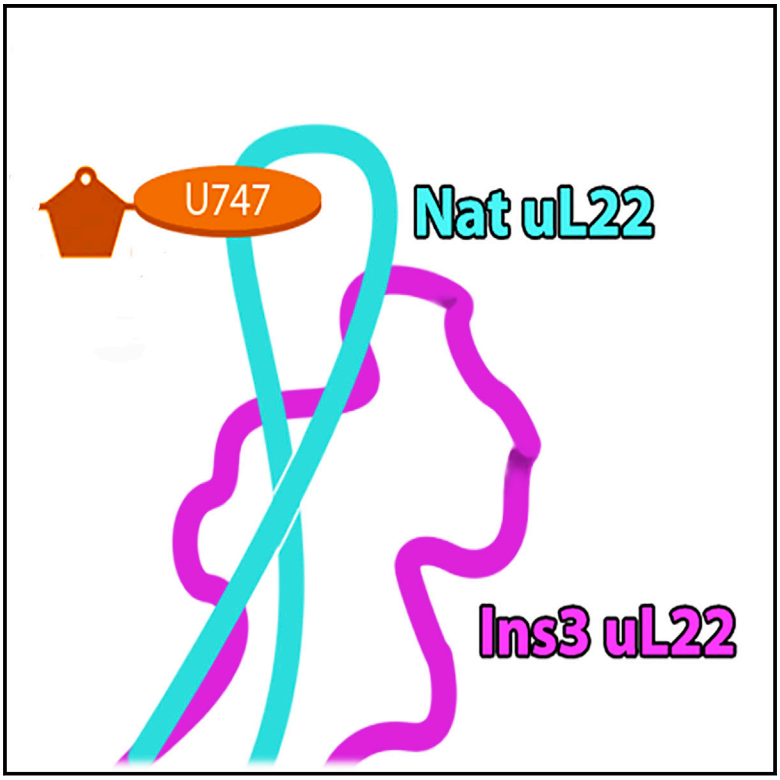

Authors

Itai Wekselman, Ella Zimmerman, Chen Davidovich, ..., Lasse Lindahl, Janice M. Zengel, Ada Yonath

Correspondence

ada.yonath@weizmann.ac.il

In Brief

Wekselman et al. report the crystal structure of the large ribosomal subunit with an insertion mutation in ribosomal protein uL22 that renders resistance to erythromycin. The mutation triggers structural rearrangements in the loop of uL22 and rRNA nucleotides in the exit tunnel that increase the flexibility of erythromycin binding pocket.

Highlights

- Structure of the 50S subunit with a distal erythromycin resistance mutation in uL22
- The mutation triggers substantial conformational changes in the exit tunnel
- The rRNA rearrangements propagate to the binding pocket of erythromycin

Wekselman et al., 2017, Structure *25*, 1233–1241
August 1, 2017
http://dx.doi.org/10.1016/j.str.2017.06.004

CellPress

Structure
Article

The Ribosomal Protein uL22 Modulates the Shape of the Protein Exit Tunnel

Itai Wekselman,[1] Ella Zimmerman,[1] Chen Davidovich,[1] Matthew Belousoff,[1] Donna Matzov,[1] Miri Krupkin,[1] Haim Rozenberg,[1] Anat Bashan,[1] Gilgi Friedlander,[2] Jette Kjeldgaard,[3] Hanne Ingmer,[3] Lasse Lindahl,[4] Janice M. Zengel,[4] and Ada Yonath[1,5,*]

[1]Department of Structural Biology, The Weizmann Institute of Science, Rehovot 7610001, Israel
[2]The Ilana and Pascal Mantoux Institute for Bioinformatics, The Nancy and Stephen Grand Israel National Center for Personalized Medicine, Weizmann Institute of Science, Rehovot 7610001, Israel
[3]Department of Veterinary Disease Biology, University of Copenhagen, 1870 Frederiksbergc, Denmark
[4]Department of Biological Sciences, University of Maryland, Baltimore County, Baltimore, MD 21250, USA
[5]Lead Contact
*Correspondence: ada.yonath@weizmann.ac.il
http://dx.doi.org/10.1016/j.str.2017.06.004

SUMMARY

Erythromycin is a clinically useful antibiotic that binds to an rRNA pocket in the ribosomal exit tunnel. Commonly, resistance to erythromycin is acquired by alterations of rRNA nucleotides that interact with the drug. Mutations in the β hairpin of ribosomal protein uL22, which is rather distal to the erythromycin binding site, also generate resistance to the antibiotic. We have determined the crystal structure of the large ribosomal subunit from *Deinococcus radiodurans* with a three amino acid insertion within the β hairpin of uL22 that renders resistance to erythromycin. The structure reveals a shift of the β hairpin of the mutated uL22 toward the interior of the exit tunnel, triggering a cascade of structural alterations of rRNA nucleotides that propagate to the erythromycin binding pocket. Our findings support recent studies showing that the interactions between uL22 and specific sequences within nascent chains trigger conformational rearrangements in the exit tunnel.

INTRODUCTION

Several classes of antibiotics inhibit protein synthesis by targeting functional regions in the bacterial ribosome. Examples of antibiotic targets are the peptidyl transferase center (PTC) and the ribosomal exit tunnel through which nascent proteins migrate until they exit from the ribosome. This tunnel begins adjacent to the PTC and extends through the core of the large subunit (Figure 1A). It is lined mainly by rRNA that accommodates the tips of extended internal loops of four ribosomal proteins. Among them, the tips of ribosomal proteins uL4 and uL22 form its narrowest constriction, located near its entrance (Figure 1). Biochemical, genetic, and structural studies have shown that the tunnel interacts with specific sequence motifs of nascent chains. These interactions may lead to translation arrest that regulates gene expression (Arenz et al., 2014; Bischoff et al., 2014; Chiba et al., 2011; Gong and Yanofsky, 2003; Koch et al., 2017; Nakatogawa and Ito, 2002; Ramu et al., 2011; Seidelt et al., 2009; Sohmen et al., 2015; Vazquez-Laslop et al., 2011; Woolhead et al., 2006).

Erythromycin (Ery) was the first member of the macrolide family of antibiotics to be used in clinical therapy (McGuire et al., 1952). Ery, as all other macrolides studied so far, binds with a high affinity to a pocket located in the tunnel wall near its entrance (Figure 1B), which is composed solely of nucleotides in domain V of 23S rRNA (Bulkley et al., 2010; Dunkle et al., 2010; Schlunzen et al., 2001). Previous studies have demonstrated that Ery inhibits protein synthesis and triggers the release of short peptidyl-tRNA (Otaka and Kaji, 1975). Based on these findings, it was assumed that Ery inhibits the translation of proteins by simply blocking the progression of nascent chains along the exit tunnel. However, this assumption was challenged by crystal structures of ribosomes in complex with Ery, which demonstrate that the antibiotic does not completely block the exit tunnel (Bulkley et al., 2010; Dunkle et al., 2010; Schlunzen et al., 2001; Tu et al., 2005), as well as by a series of biochemical findings, showing that specific proteins can be actively translated by bacteria in the presence of a high concentration of Ery (Kannan et al., 2012). Furthermore, genome-wide ribosome profiling experiments have demonstrated that, in the presence of Ery, the identity of amino acids residues of the nascent chain in the C terminus of the peptidy-tRNA and the upcoming aminoacyl-tRNA determine the arrest point of the translation process. According to the current view, Ery inhibits protein synthesis by hindering the formation of the peptide bond between specific substrates in the PTC (Davis et al., 2014; Kannan et al., 2014; Sothiselvam et al., 2016).

Resistance to Ery can be triggered by methylation of the rRNA nucleotide A2058 (*Escherichia coli* numbering is used throughout for rRNA nucleotides) in the antibiotic binding pocket or by its mutation to guanine (Meier et al., 1994; Skinner et al., 1983). Mutations of other rRNA nucleotides that interact directly with Ery also bestow resistance (Canu et al., 2002; Pfister et al., 2004). In addition, it has been known for over 40 years that mutations in two ribosomal proteins, uL22 and uL4, confer resistance or reduce susceptibility to Ery (Pardo and Rosset, 1977; Wittmann et al., 1973). The first characterized mutation in uL22 that renders resistance to Ery was the deletion of three residues

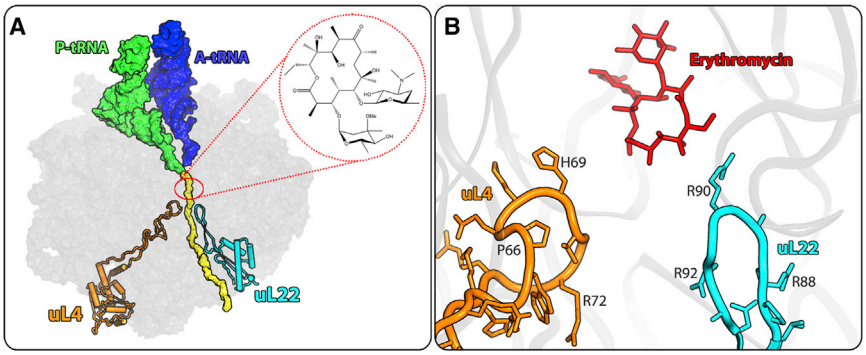

Figure 1. The Nascent Chain Exit Tunnel

(A) A section through the large ribosomal subunit of *T. thermophilus* (PDB: 4V5D, Voorhees et al., 2009) with the crystallographic determined positions of A-site (blue) and P-site (green) tRNAs. A modeled-poly alanine nascent chain is shown in yellow and the ribosomal proteins uL4 and uL22 are shown in orange and cyan, respectively. The approximate location of the Ery binding pocket is indicated as a red circle.

(B) A view of the region of the exit tunnel indicated by the red circle in (A) derived from the *T. thermophilus* 70S crystal structure in complex with Ery (PDB: 4V7X, Bulkley et al., 2010). The tips of the ribosomal proteins uL4 and uL22 are shown in orange and cyan, respectively; Ery is shown in red and the rRNA in gray.

at positions 82–84 of the protein in *E. coli* (Δ82–84) (Chittum and Champney, 1994; Wittmann et al., 1973). Additional mutations have been identified in uL22 that are associated with resistance to macrolides in *E. coli, Staphylococcus aureus, Streptococcus pneumoniae, Streptococcus pyogenes, Helicobacter pylori, Haemophilus influenza*, and *Francisella tularensis* (Binh et al., 2014; Canu et al., 2004; Clark et al., 2002; Diner and Hayes, 2009; Gestin et al., 2010; Malbruny et al., 2002a, 2002b; Pihlajamaki et al., 2003; Zaman et al., 2007). These mutations, which include a variety of deletions, insertions, and single amino acid substitutions, are mapped to the β hairpin loop that extends from the globular domain of uL22 and reaches the tunnel wall (Figure 1A). Interestingly, in many cases ribosomes with mutations in uL22 that confer resistance to Ery bind the drug with high affinity (Lovmar et al., 2009; Wittmann et al., 1973; Zaman et al., 2007).

The structures of ribosomes in complex with Ery indicate that the closest distance of the bound antibiotic to uL22 is ~9 Å (Bulkley et al., 2010; Dunkle et al., 2010; Schlunzen et al., 2001; Tu et al., 2005); this distance precludes a direct chemical interaction between the protein and the antibiotic. Therefore, the resistance to Ery acquired by mutations in uL22 was considered to occur indirectly by altering the conformation of the 23S rRNA (Schlunzen et al., 2001). Studies based on cryoelectron microscopy (cryo-EM) at low resolution have suggested that the Ery resistance of the Δ82–84 mutant is related to an increase in the diameter of the protein exit tunnel (Gabashvili et al., 2001). Also, comparison between the crystal structures of *Thermus thermophilus* uL22 containing the Δ82–84 mutation with that of uL22 of *Deinococcus radiodurans* suggests that the β hairpin of the mutant is shifted into the lumen of the ribosome exit tunnel and thus may alter the conformation of the surrounding 23S rRNA nucleotides (Berisio et al., 2003; Davydova et al., 2002). Interestingly, the crystal structure of the archaeon *Haloarcula marismortui* large ribosomal subunit with the equivalent Δ82–84 mutation (Tu et al., 2005) also indicates that the mutation triggers a shift in the positions of the β hairpin loop of uL22 and of a few rRNA nucleotides. However, these structural changes do not propagate to the Ery binding pocket.

Here, we report the X-ray crystal structures of the large ribosomal subunit from the eubacterium *D. radiodurans* containing an insertion of three residues in uL22 that renders resistance to Ery and of its complex with the antibiotic. These structures reveal that the mutation triggers structural rearrangements in the β hairpin loop of uL22 and in rRNA nucleotides in the tunnel wall that consequently increase the flexibility of the Ery binding pocket. We also present supporting analysis of a deletion mutation in uL22 of the Gram-positive pathogen *S. aureus* that

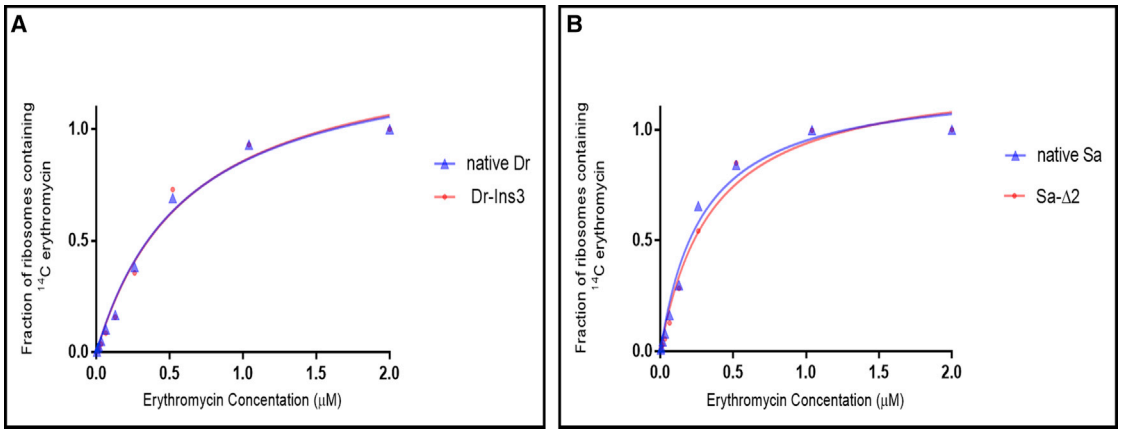

Figure 2. Ery Binding to uL22 Mutants

Determination of Ery equilibrium dissociation constants for the Dr-Ins3 (A) and Sa-Δ2 (B) large ribosomal subunits.

Table 1. Crystallographic Data and Refinement Statistics for the D50S-Ins3 and D50S-In3Ery Structures

	D50S- Ins3	D50S- Ins3Ery
Data Collection		
Space group	I222	I222
Cell parameters		
a, *b*, *c* (Å)	169.7, 412.5, 697.0	170.1, 411.6, 696.0
X-ray source	ID23-2, ESRF	ID23-2, ESRF
Detector	MarCCD 225	MarCCD 225
Wavelength (Å)	0.873	0.873
No. of crystals	11	10
Resolution (Å)	50–3.65 (3.71–3.65)	50–3.54 (3.6–3.54)
No. of observed reflections	1,325,630	1,344,521
No. of unique reflections	261,274	270,450
Redundancy	5.1 (4.4)	5 (4.4)
Completeness (%)	95.9 (92.1)	91 (90.3)
$\langle I \rangle / \langle \sigma \rangle$	7.3 (1.43)	8.3 (1.57)
R-merge (%)	18.8 (80.6)	16.4 (81.8)
Refinement		
R factor (%)	22.57	23.4
R-free (5%)	27.0	28.23
RMSD		
Bond lengths (Å)	0.007	0.007
Bond angles (°)	1.2	1.2

Figures in parentheses are given for the highest-resolution bin. RMSD, root-mean-square deviation.

triggers resistance to Ery. Based on our results and recent studies obtained elsewhere (Bischoff et al., 2014; Sohmen et al., 2015; Zhang et al., 2015), we propose a feasible explanation for the resistance mechanism of this mutant as well as for the involvement of uL22 in translation arrest.

RESULTS AND DISCUSSION

Analysis of the uL22 Mutants

To investigate the uL22-mediated resistance to Ery we isolated and characterized two spontaneous Ery-resistant mutants: One carries an insertion of three residues (Val, Pro, and Arg) after Arg88 (*E. coli* numbering is used throughout for uL22 residues) in *D. radiodurans* uL22 (Dr-Ins3) and another with deletion of two residues (Arg88 and Ala89) in *S. aureus* uL22 (Sa-Δ2). The minimal inhibitory concentration values of Ery for Dr-Ins3 and Sa-Δ2 are 8- and 16-fold higher, respectively than those observed for the wild-type strains. We have used a filter binding assay with ^{14}C radiolabeled Ery to determine whether these mutations reduce the affinity of Ery to the bacterial ribosome (Figure 2). The dissociation constant (K_D) for Ery binding to the Dr-Ins3 large ribosomal subunit is identical to the one observed for the native subunit (0.6 ± 0.1 μM). The K_D values of Ery binding to the Sa-Δ2 and wild-type large ribosomal subunits are comparable (0.35 ± 0.05 and 0.3 ± 0.05 μM, respectively).

The Insertion Mutation in uL22 Triggers Structural Rearrangements in the Wall of the Exit Tunnel

We have determined the crystal structure of the *D. radiodurans* large ribosomal subunit (D50S) containing the Dr-Ins3 mutation (D50S-Ins3) at a resolution of 3.65 Å (Table 1). The unbiased weighted $2F_o - F_c$ electron density map indicates that the uL22 β hairpin loop is shifted from the wall toward the interior of the nascent chain exit tunnel (Figures 3A and 3B). Following this conformational change, the backbone of uL22 Arg88 is shifted by 13.5 Å. The mutation disrupts the twisted conformation of the β hairpin and increases the maximal width of the loop from 5.5 to 9 Å. The altered conformation of the loop is stabilized by interactions with rRNA nucleotides that are mainly located on one side of the tunnel wall. As a result, the part of the loop found in the lumen of the tunnel seems to be flexible and should not disrupt the progression of the nascent chain.

The displacement of the uL22 loop induces a shift in the position of a number of rRNA nucleotides (Figure 3C). The most notable structural rearrangements occur at the position of the U747 base, which rotates toward the space that in the native structure is occupied by the tip of the uL22 loop. In native D50S, U747 is stacked against U2613 and bridges 23S rRNA domains II and V together. The altered position of U747 triggers, in turn, conformational changes in U2613 and C2612: the phosphate backbone of U2613 is shifted by 3.5 Å while the base of C2612 rotates by 65°.

U2611, the adjacent nucleotide in the chain, is located in the Ery binding pocket. The conformation of U2611 in D50S-Ins3 is similar to that observed in the native D50S structure. However, trace density in the vicinity of U2611 demonstrates that it adopts at least one additional conformation that is shifted toward the lumen of the exit tunnel (Figure 3D). A2062 is a flexible nucleotide that is also located in the Ery binding pocket. The electron density maps demonstrate that, in addition to the native conformation, A2062 adopts alternate conformations that protrude into the lumen of the exit tunnel. Although the current resolution is not sufficient for accurate determination of the altered conformations of U2611 and A2062, we estimate that the distance between these two nucleotides can reach 3–4 Å, which is suitable for direct chemical interactions (Figure 3D).

Ery Binds in a Similar Way to D50S-Ins3 and Native Ribosomes

To find out if the structural changes that are induced by the Ins3 mutation influence the binding mode of Ery, we also determined the crystal structure of D50S-Ins3 in complex with the antibiotic (D50S-Ins3Ery) at a resolution of 3.54 Å (Table 1). The weighted $F_o - F_c$ electron density map showed unambiguously that Ery is located in its binding site near the exit tunnel entrance, as was observed in all the crystal structures of bacterial ribosomes in complex with the antibiotic (Bulkley et al., 2010; Dunkle et al., 2010; Schlunzen et al., 2001) (Figures 4A and 4B). The closest distance between the uL22 loop and Ery in D50S-In3Ery is 9 Å, which demonstrates that uL22 and the antibiotic do not directly interact.

The conformations of the rRNA nucleotides in the Ery binding pocket are very similar to those observed in the crystal structures of eubacterial ribosomes in complex with the antibiotic (Figure 4B). Some variation has been observed in the conformation

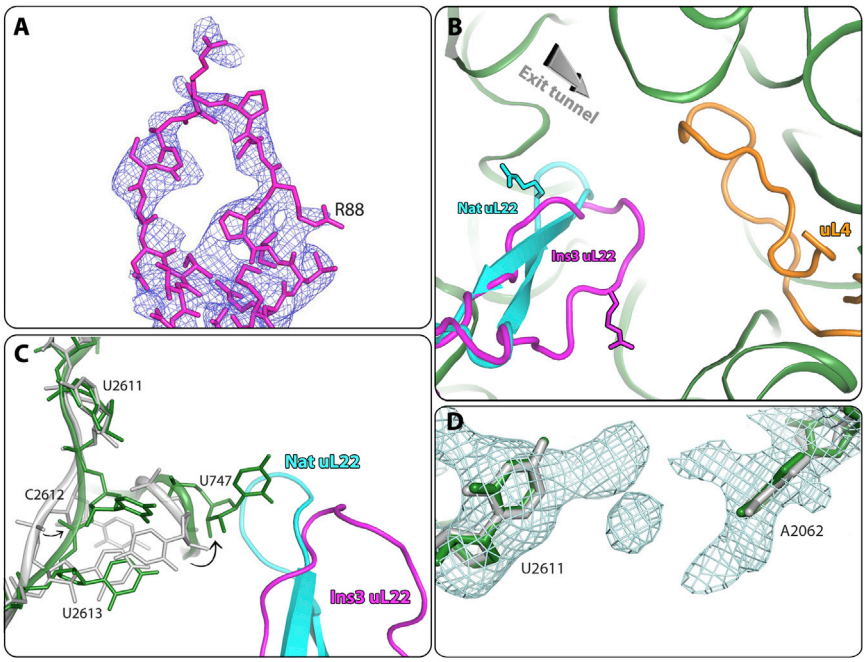

Figure 3. The Structural Rearrangements in the Exit Tunnel of D50S-Ins3

(A) The altered conformation of the uL22 loop in D50S-Ins3. The uL22 loop is shown in pink and the omit $2F_o - F_c$ electron density map (light blue) is countered at 1σ.

(B) The nascent chain exit tunnel in D50S-Ins3 showing the native (PDB: 2ZJR, cyan) and the altered (pink) conformations of the uL22 loop. The rRNA is shown in green and the uL4 protein in orange. The direction of the tunnel is indicated by the gray arrow.

(C) The structural rearrangements of rRNA nucleotides in D50S-Ins3 (green) in comparison with native D50S (gray). The tip of the native uL22 is shown in cyan and the tip of the D50S-Ins3 uL22 in pink.

(D) The alternate conformations of U2611 and A2062. The omit $2F_o - F_c$ density map around U2611 and A2062 (light blue) is countered at 1σ.

of A2062: in three of the structures (D50S-Ins3Ery, D50S in complex with Ery, and *E. coli* 70S ribosome in complex with Ery) the base of A2062 is located in the lumen of the tunnel and interacts with Ery, while in the structure of *T. thermophiles* 70S in complex with Ery it is found in close proximity to the wall of the tunnel (Figure 4B). In the D50S Ins3-Ery complex structure, U2611 and A2062 do not adopt any alternative conformations.

Structural Basis of uL22-Mediated Resistance to Ery

Our study demonstrates that an Ery resistance mutation in uL22 can initiate a cascade of structural changes that propagates to the Ery binding pocket.

In the D50S-Ins3 structure the β hairpin loop of uL22 shifts from the wall toward the lumen of the nascent chain exit tunnel. The altered conformation of the loop triggers a cascade of structural changes among rRNA nucleotides that is relayed to the Ery binding pocket (Figure 3). As part of these structural rearrangements U2611 and A2062, located in the binding pocket of the antibiotic, adopt alternate conformations. The flexibility of U2611 demonstrates that its conformation is readily affected by structural rearrangements of the rRNA nucleotides in its vicinity. A2062 is a highly flexible nucleotide that adopts different conformations in various ribosomal crystal structures (Belousoff et al., 2011; Bulkley et al., 2010; Dunkle et al., 2010; Harms et al., 2004; Schmeing et al., 2005; Tu et al., 2005).

In the D50S-Ins3Ery complex structure, no conformational changes were observed in U2611 and A2062 or in any other rRNA nucleotides in the binding pocket of Ery (Figure 4). These observations are in agreement with our finding that the Ins3 mutation does not lower the affinity of Ery to the large ribosomal subunit (Figure 2). Recent studies have shown that a distinct set of proteins can be translated by Ery-bound ribosomes. It was suggested that some of these polypeptides can bypass the antibiotic by stabilizing A2062 in a conformation that increases the space available for the passage of nascent chains (Kannan et al., 2012). We propose that, when Ery is bound to the mutated ribosomes, the nascent peptide may alter the conformation of the flexible nucleotides U2611 and A2062 in a way that facilitates its progression through the exit tunnel.

The Dr-Ins3 mutation is located after Arg88, at the tip of the native uL22 loop. A similar Ery resistance mutation, an insertion of Val, Arg, Pro, and Arg, was identified in uL22 of

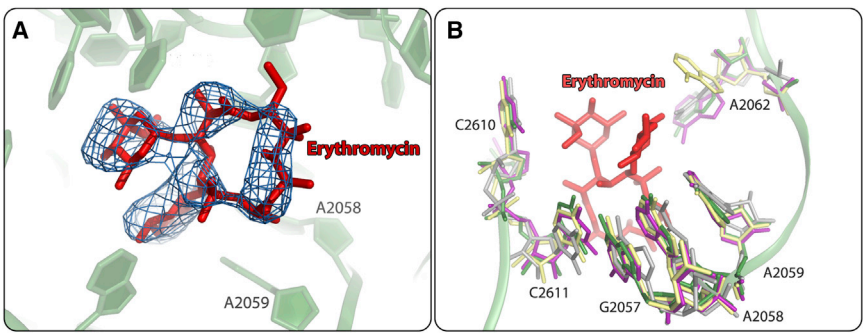

Figure 4. The Binding of Ery to D50S-Ins3

(A) The Ery binding pocket in D50S-Ins3Ery. The rRNA backbone is shown in green; Ery is shown in red, and the 2.5σ omit $F_o - F_c$ electron density map in blue.

(B) A comparison between the Ery binding pocket in D50S-Ins3Ery (Ery in red and rRNA in green) and those observed in D50S in complex with Ery (PDB: 1JZY, Schlunzen et al., 2001; the rRNA is in gray), the 70S *T. thermophilus* ribosome in complex with Ery (PDB: 4V7X, Bulkley et al., 2010; the rRNA is in yellow) and the *E. coli* 70S ribosome in complex with Ery (PDB: 4V7U, Dunkle et al., 2010; the rRNA is in purple).

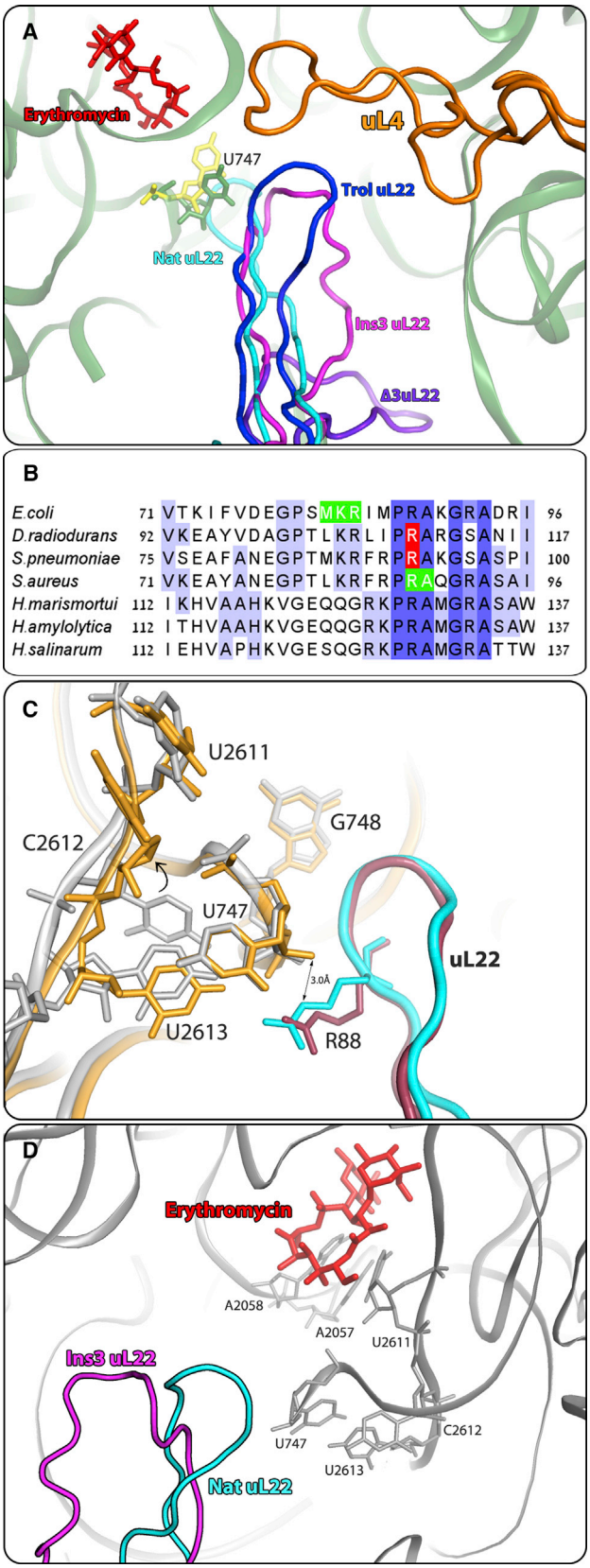

Figure 5. Mechanism of uL22-Mediated Ery Resistance

(A) Comparison between the different conformations of uL22 in native D50S (PDB: 2ZRR, cyan), D50S-Ins3Ery (pink), D50S-Trol (PDB: 1OND, Berisio et al., 2003; blue) and H50S-Δ3 (PDB: 1YJ9, Tu et al., 2005; purple). The rRNA backbone, the uL4 protein, and Ery of D50S-Ins3Ery are shown in green, orange and red, respectively. The positions of U747 in D50S-Ins3Ery and H50S-Δ3 are shown in green and yellow, respectively.

(B) Sequence alignment of uL22 from eubacteria (*E. coli*, *S. aureus, S. pneumoniae*, and *D. radiodurans*) and archaea (*H. marismortui, H. amylolytica*, and *H. salinarum*). The positions of the deletion (Δ82–84, Sa-Δ2) and insertion (Dr-Ins3, Sp-Ins4) mutations are marked in green and red, respectively.

(C) Overlay of the structures of D50S (PDB: 2ZJR) and *S. aureus* large ribosomal subunit (SA50S) (PDB: 4WCE, Eyal et al., 2015). The rRNA of D50S and SA50S is shown in gray and orange, respectively. The tip of the uL22 loop in D50S and SA50S is shown in cyan and red, respectively.

(D) Structural rearrangements in uL22 may induce substantial conformation changes in the Ery binding pocket by disrupting the U2611–2057 base-pair. The rRNA of native D50S and Ery of the D50S-Ins3Ery complex are shown in gray and red, respectively.

the Gram-positive pathogen *S. pneumoniae* (Sp-Ins4) (Pihlajamaki et al., 2003). Sequence alignment between uL22 of *D. radiodurans, S. aureus*, and *S. pneumoniae* indicates that the Sa-Δ2, Sp-Ins4, and Dr-Ins3 mutations are found at equivalent positions (Figure 5B). Interestingly, a high number of mutations that render resistance to Ery have been identified in the Arg88-Ala93 segment of uL22 (Diner and Hayes, 2009). The interactions of the highly conserved Arg88 with the phosphate backbone of G748 and the sugar of U747 stabilize the native conformation of uL22 (Figure 5C). Mutations in uL22 that would disrupt these interactions are likely to induce substantial structural changes in the β hairpin loop of the protein.

The rRNA nucleotides U747, U2613, and C2612 that alter their conformation in D50S-In3 are highly conserved in eubacteria (>98%) (Cannone et al., 2002). In *S. aureus, S. pneumoniae*, and most eubacteria the rRNA nucleotide at position 2611 is C, but in others (including *D. radiodurans*) it is U. A comparison of between D50S and the crystal structure of *S. aureus* large ribosomal subunit in this region demonstrates that the loop of uL22 and the rRNA both adopt similar conformations (Figure 5C) (Eyal et al., 2015). One significant structural difference is observed at the base of C2612, which points to opposite directions in the two structures. As a result some of the structural changes among rRNA nucleotides that are induced by the displacement of uL22 may be species specific.

In contrast to Dr-Ins3 and Sa-Δ2, some mutations in uL22 that trigger resistance to Ery decrease the affinity of the antibiotic to the bacterial ribosome substantially (Diner and Hayes, 2009; Lovmar et al., 2009; Zaman et al., 2007). It is reasonable that these mutations alter the conformation of uL22 and induce a longer cascade of structural rearrangements among rRNA nucleotides that changes the structure of the Ery binding pocket. For example, a shift in the position of U2611 can disrupt the 2611–2057 base pair and induce conformational changes that propagate to A2058 and A2059 (Figure 5D).

It was suggested that the altered conformation of uL22 in the Δ82–84 mutant decreases the rate of the transport of Ery through the exit tunnel to its binding pocket (Lovmar et al., 2009). Another study has proposed that the Δ82–84 mutation renders resistance to Ery by changing the translation level of some proteins that participate in the uptake of the antibiotic (Moore and Sauer,

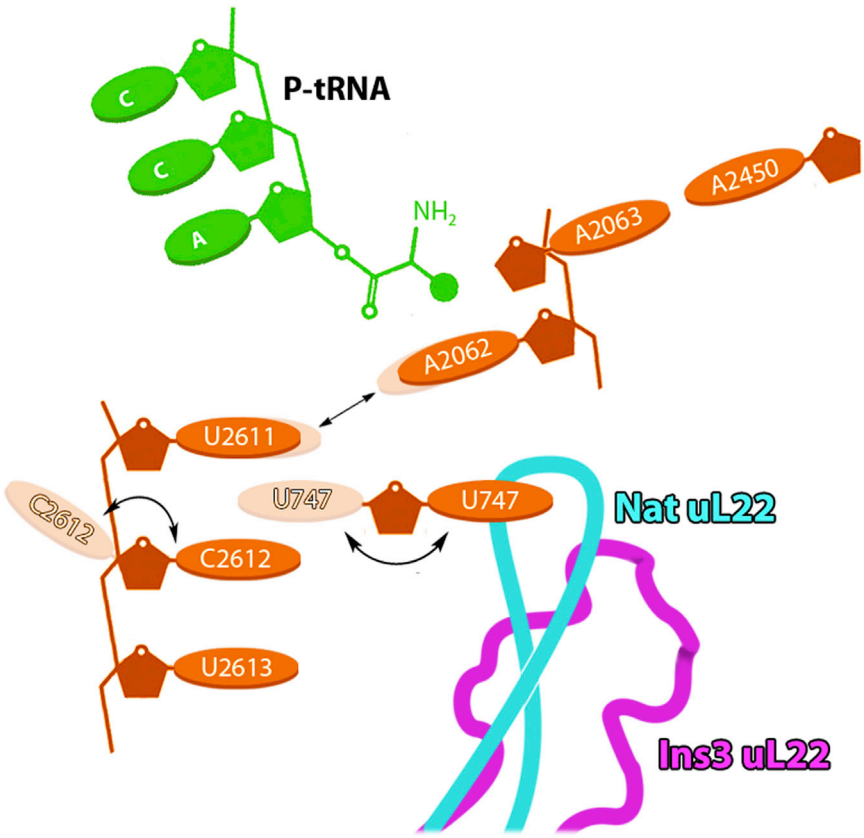

Figure 6. Schematic Representation of a Proposed Relay Mechanism between uL22 and the PTC that Contributes to Translation Stalling

The native and Ins3 conformations of uL22 are shown in cyan and pink, respectively. The rRNA nucleotides are marked in orange and the P-tRNA is shown in green.

2008). It cannot be excluded that these suggested mechanisms, together with the structural changes in the binding pocket of Ery, contribute to the observed resistance mechanism to the antibiotic.

Comparison between D50S-Ins3 and Previous Determined Structures of Ribosomes with Altered uL22 Conformations

The crystal structure of a *H. marismortui* large ribosomal subunit with Δ82–84 in uL22 (H50S-Δ3) demonstrates that the mutation triggers a shift in the position of the uL22 hairpin loop: it is located deeper in the tunnel and its orientation is perpendicular to the position of the uL22 loop in D50S-Ins3 (Tu et al., 2005). The conformation of the rRNA nucleotide U747 in H50S-Δ3 is similar to that observed in D50S-Ins3 (Figure 5A). However, in H50S-Δ3 the displacement of U747 does not trigger a cascade of structural changes in additional rRNA nucleotides that propagates to the Ery binding pocket. The Δ82–84 mutation decreases the affinity of Ery to the ribosome by 5-fold (Lovmar et al., 2009). This observation indicates that the mutation induces structural changes in the binding pocket of the antibiotic. It should be noted that Ery does not bind to archaeal ribosomes because they possess guanine in position 2058, as in eukaryotes, whereas in eubacteria position 2058 is adenine. As in this region of uL22 the sequence is not conserved between archaea and eubacteria (Figure 5B) (Wilson et al., 2005), it is unclear whether the Δ82–84 mutation triggers similar structural changes in eubacteria.

Troleandomycin (Trol) is a semi-synthetic macrolide derivative that is bulkier than Ery since all of its hydroxyl groups are either methylated or acetylated. In the crystal structure of D50S in complex with Trol (D50S-Trol), the binding of the antibiotic triggers a shift of the entire tip of the uL22 β hairpin (11 amino acids) across the tunnel (Figure 5A) (Berisio et al., 2003). In D50S-Trol, the structural rearrangements in uL22 do not alter the conformation of rRNA nucleotides in the wall of the exit tunnel. Collectively, the D50S-Trol, D50S-Ins3, and H50S-Δ3 crystal structures demonstrate that the β hairpin loop of uL22 is highly flexible and can adopt diverse conformations.

The D50S-Ins3 Structure May Provide Additional Insights on the Role of uL22 in Translation Arrest

One interesting example of the regulatory properties of the exit tunnel is that specific sequences in nascent peptides can trigger translation arrest. Genetic, biochemical, and structural studies demonstrate that uL22, uL4, and a few rRNA nucleotides located at the segment between the tunnel entrance and its constriction may respond to the arrest sequence (Arenz et al., 2014; Bhushan et al., 2011; Bischoff et al., 2014; Chiba et al., 2011; Lawrence et al., 2008; Nakatogawa and Ito, 2002; Seidelt et al., 2009; Sohmen et al., 2015; Vazquez-Laslop et al., 2010, 2011). The current model of ribosome stalling indicates that specific interactions of the nascent chain with the exit tunnel trigger structural changes in the PTC which inhibit peptide bond formation. The stalling signal can be relayed to the PTC by structural rearrangements in the nascent chain and/or the exit tunnel (Bischoff et al., 2014; Koch et al., 2017; Wilson et al., 2016).

The recently published cryo-EM structures of TnaC, MifM, and SecM stalled ribosomes demonstrate that the interaction between these three peptides and the β hairpin loop of uL22 is essential for translation stalling (Bischoff et al., 2014; Sohmen et al., 2015; Zhang et al., 2015). Interestingly, MifM induces translation stalling in *Bacillus subtilis* but not in *E. coli*. It was shown that the identity of a single amino acid within uL22 (residue 90) dictates the species specificity of MifM (Sohmen et al., 2015). This finding demonstrates that even minor conformational changes in uL22 can have a major influence on translation arrest.

The rRNA nucleotide A2062 has been identified as one of the tunnel sensors that has a key role in the translation arrest mechanism (Arenz et al., 2014; Seidelt et al., 2009; Vazquez-Laslop et al., 2008; Zhang et al., 2015). As mentioned above, the base

of A2062 is highly flexible and can adopt diverse conformations. It was suggested that the flexibility of A2062 is important for the relay of the arrest signal from the exit tunnel to the PTC as it is located in an ideal position at the entrance of the tunnel to interact with the nascent chain (Vazquez-Laslop et al., 2008, 2010). The structural changes may propagate to the PTC from A2062, through its neighboring nucleotide, C2063 (Figure 6) (Chirkova et al., 2010; Koch et al., 2017; Sothiselvam et al., 2014).

The D50S-Ins3 structure demonstrates that conformational changes in uL22 can trigger a cascade of structural alterations among rRNA nucleotides that propagates to A2062. Although in the current cryo-EM structures of stalled ribosomes no substantial conformational changes were observed in uL22, we suggest that the interactions of different arrest peptides with uL22 may alter the conformation of its β hairpin and trigger a cascade of structural changes among the nascent chain and rRNA nucleotides in the tunnel wall that propagates to the PTC through A2062 (Figure 6).

STAR★METHODS

Detailed methods are provided in the online version of this paper and include the following:

- KEY RESOURCES TABLE
- CONTACT FOR REAGENT AND RESOURCE SHARING
- EXPERIMENTAL MODEL AND SUBJECT DETAILS
  - Isolation of the Erythromycin Resistant Mutants
- METHOD DETAILS
  - Bacterial Growth
  - Purification of the Large Ribosomal Subunit
  - Erythromycin Binding
  - Crystallization
  - Data Collection and Processing
  - Structure Solution, Model Building and Refinement
  - Figure Generation and Sequence Alignment
- QUANTIFICATION AND STATISTICAL ANALYSIS
- DATA AND SOFTWARE AVAILABILITY

AUTHOR CONTRIBUTIONS

I.W., A.B., H.I., L.L., J.Z., and A.Y. designed the research. I.W., C.D., M.B., D.M., M.K., E.Z., H.R., A.B., J.Z., and J.K. performed the research; I.W., G.F., and A.B. analyzed the data; I.W., A.B., and A.Y. wrote the paper.

ACKNOWLEDGMENTS

We thank all of the current and former members of the ribosome group at the Weizmann Institute of Science who assisted in different stages of this project: Moshe Peretz, Tamar Auerbach, Maggie Kessler, Miriam Lashever, Shosh Tel-Or, Yakov Halfon, Dina Levy, Yehuda Halfon, Tal Shapira, Giuseppe Cimicata, Zohar Eyal, and Tamara Litwin. We also wish to express our gratitude to Ghil Jona and Amnon Naziri from the Weizmann Bacteriology Unit for performing the large-scale fermentations of the Dr-3 mutant. We are thankful to Henrik Westh (Hvidovre University Hospital) and the Crown Institute of Genomics (The Nancy and Stephen Grand Israel National Center for Personalized Medicine) for sequencing the genomes of the Sa-Δ2 and Dr-3 mutants, respectively. X-ray diffraction data were collected at beamline ID23-2 at the European Synchrotron Radiation Facility, Grenoble, France. Funds were provided to A.Y. by the European Research Council (grant 322581-NOVRIB), the Merieux Research grant and the Kimmelman Center for Macromolecular Assemblies. A.Y. holds the Martin and Helen Kimmel Professional chair. M.K was supported by the Adams Fellowship Program of the Israel Academy of Sciences and Humanities. G.F. is the Incumbent of the David and Stacey Cynamon Research fellow Chair in Genetics and Personalized Medicine. J.Z. and L.L. were supported by grant MCB 0349943 from the National Science Foundation. J.K. is supported by the Bent Thorberg Foundation.

Received: May 25, 2016
Revised: May 8, 2017
Accepted: June 2, 2017
Published: July 6, 2017

REFERENCES

Adams, P.D., Afonine, P.V., Bunkoczi, G., Chen, V.B., Davis, I.W., Echols, N., Headd, J.J., Hung, L.W., Kapral, G.J., Grosse-Kunstleve, R.W., et al. (2010). PHENIX: a comprehensive Python-based system for macromolecular structure solution. Acta Crystallogr. D Biol. Crystallogr. *66*, 213–221.

Arenz, S., Meydan, S., Starosta, A.L., Berninghausen, O., Beckmann, R., Vazquez-Laslop, N., and Wilson, D.N. (2014). Drug sensing by the ribosome induces translational arrest via active site perturbation. Mol. Cell *56*, 446–452.

Belousoff, M.J., Shapira, T., Bashan, A., Zimmerman, E., Rozenberg, H., Arakawa, K., Kinashi, H., and Yonath, A. (2011). Crystal structure of the synergistic antibiotic pair, lankamycin and lankacidin, in complex with the large ribosomal subunit. Proc. Natl. Acad. Sci. USA *108*, 2717–2722.

Berisio, R., Schluenzen, F., Harms, J., Bashan, A., Auerbach, T., Baram, D., and Yonath, A. (2003). Structural insight into the role of the ribosomal tunnel in cellular regulation. Nat. Struct. Biol. *10*, 366–370.

Bhushan, S., Hoffmann, T., Seidelt, B., Frauenfeld, J., Mielke, T., Berninghausen, O., Wilson, D.N., and Beckmann, R. (2011). SecM-stalled ribosomes adopt an altered geometry at the peptidyl transferase center. PLoS Biol. *9*, e1000581.

Binh, T.T., Shiota, S., Suzuki, R., Matsuda, M., Trang, T.T.H., Kwon, D.H., Iwatani, S., and Yamaoka, Y. (2014). Discovery of novel mutations for clarithromycin resistance in *Helicobacter pylori* by using next-generation sequencing. J. Antimicrob. Chemother. *69*, 1796–1803.

Bischoff, L., Berninghausen, O., and Beckmann, R. (2014). Molecular basis for the ribosome functioning as an L-tryptophan sensor. Cell Rep. *9*, 469–475.

Bulkley, D., Innis, C.A., Blaha, G., and Steitz, T.A. (2010). Revisiting the structures of several antibiotics bound to the bacterial ribosome. Proc. Natl. Acad. Sci. USA *107*, 17158–17163.

Cannone, J.J., Subramanian, S., Schnare, M.N., Collett, J.R., D'Souza, L.M., Du, Y., Feng, B., Lin, N., Madabusi, L.V., Muller, K.M., et al. (2002). The comparative RNA web (CRW) site: an online database of comparative sequence and structure information for ribosomal, intron, and other RNAs. BMC Bioinformatics *3*, 2.

Canu, A., Malbruny, B., Coquemont, M., Davies, T.A., Appelbaum, P.C., and Leclercq, R. (2002). Diversity of ribosomal mutations conferring resistance to macrolides, clindamycin, streptogramin, and telithromycin in *Streptococcus pneumoniae*. Antimicrob. Agents Chemother. *46*, 125–131.

Canu, A., Abbas, A., Malbruny, B., Sichel, F., and Leclercq, R. (2004). Denaturing high-performance liquid chromatography detection of ribosomal mutations conferring macrolide resistance in Gram-positive cocci. Antimicrob. Agents Chemother. *48*, 297–304.

Chiba, S., Kanamori, T., Ueda, T., Akiyama, Y., Pogliano, K., and Ito, K. (2011). Recruitment of a species-specific translational arrest module to monitor different cellular processes. Proc. Natl. Acad. Sci. USA *108*, 6073–6078.

Chirkova, A., Erlacher, M.D., Clementi, N., Zywicki, M., Aigner, M., and Polacek, N. (2010). The role of the universally conserved A2450-C2063 base pair in the ribosomal peptidyl transferase center. Nucleic Acids Res. *38*, 4844–4855.

Chittum, H.S., and Champney, W.S. (1994). Ribosomal-protein gene sequence changes in erythromycin-resistant mutants of *Escherichia coli*. J. Bacteriol. *176*, 6192–6198.

Clamp, M., Cuff, J., Searle, S.M., and Barton, G.J. (2004). The Jalview Java alignment editor. Bioinformatics *20*, 426–427.

Clark, C., Bozdogan, B., Peric, M., Dewasse, B., Jacobs, M.R., and Appelbaum, P.C. (2002). In vitro selection of resistance in *Haemophilus influenzae* by amoxicillin-clavulanate, cefpodoxime, cefprozil, azithromycin, and clarithromycin. Antimicrob. Agents Chemother. *46*, 2956–2962.

Davis, A.R., Gohara, D.W., and Yap, M.N.F. (2014). Sequence selectivity of macrolide-induced translational attenuation. Proc. Natl. Acad. Sci. USA *111*, 15379–15384.

Davydova, N., Streltsov, V., Wilce, M., Liljas, A., and Garber, M. (2002). L22 ribosomal protein and effect of its mutation on ribosome resistance to erythromycin. J. Mol. Biol. *322*, 635–644.

DeLano, W.L. (2002). The Pymol Molecular Graphics System (Delano Scientific).

Diner, E.J., and Hayes, C.S. (2009). Recombineering reveals a diverse collection of ribosomal proteins L4 and L22 that confer resistance to macrolide antibiotics. J. Mol. Biol. *386*, 300–315.

Dunkle, J.A., Xiong, L., Mankin, A.S., and Cate, J.H. (2010). Structures of the *Escherichia coli* ribosome with antibiotics bound near the peptidyl transferase center explain spectra of drug action. Proc. Natl. Acad. Sci. USA *107*, 17152–17157.

Emsley, P., Lohkamp, B., Scott, W.G., and Cowtan, K. (2010). Features and development of Coot. Acta Crystallogr. D Biol. Crystallogr. *66*, 486–501.

Eyal, Z., Matzov, D., Krupkin, M., Wekselman, I., Paukner, S., Zimmerman, E., Rozenberg, H., Bashan, A., and Yonath, A. (2015). Structural insights into species-specific features of the ribosome from the pathogen *Staphylococcus aureus*. Proc. Natl. Acad. Sci. USA *112*, E5805–E5814.

Gabashvili, I.S., Gregory, S.T., Valle, M., Grassucci, R., Worbs, M., Wahl, M.C., Dahlberg, A.E., and Frank, J. (2001). The polypeptide tunnel system in the ribosome and its gating in erythromycin resistance mutants of L4 and L22. Mol. Cell *8*, 181–188.

Gestin, B., Valade, E., Thibault, F., Schneider, D., and Maurin, M. (2010). Phenotypic and genetic characterization of macrolide resistance in *Francisella tularensis* subsp. holarctica biovar I. J. Antimicrob. Chemother. *65*, 2359–2367.

Gong, F., and Yanofsky, C. (2003). A transcriptional pause synchronizes translation with transcription in the tryptophanase operon leader region. J. Bacteriol. *185*, 6472–6476.

Harms, J., Schluenzen, F., Zarivach, R., Bashan, A., Gat, S., Agmon, I., Bartels, H., Franceschi, F., and Yonath, A. (2001). High resolution structure of the large ribosomal subunit from a mesophilic eubacterium. Cell *107*, 679–688.

Harms, J.M., Schlunzen, F., Fucini, P., Bartels, H., and Yonath, A. (2004). Alterations at the peptidyl transferase centre of the ribosome induced by the synergistic action of the streptogramins dalfopristin and quinupristin. BMC Biol. *2*, 4.

Kannan, K., Vazquez-Laslop, N., and Mankin, A.S. (2012). Selective protein synthesis by ribosomes with a drug-obstructed exit tunnel. Cell *151*, 508–520.

Kannan, K., Kanabar, P., Schryer, D., Florin, T., Oh, E., Bahroos, N., Tenson, T., Weissman, J.S., and Mankin, A.S. (2014). The general mode of translation inhibition by macrolide antibiotics. Proc. Natl. Acad. Sci. USA *111*, 15958–15963.

Koch, M., Willi, J., Pradere, U., Hall, J., and Polacek, N. (2017). Critical 23S rRNA interactions for macrolide-dependent ribosome stalling on the ErmCL nascent peptide chain. Nucleic Acids Res. http://dx.doi.org/10.1093/nar/gkx195.

Lawrence, M.G., Lindahl, L., and Zengel, J.M. (2008). Effects on translation pausing of alterations in protein and RNA components of the ribosome exit tunnel. J. Bacteriol. *190*, 5862–5869.

Lovmar, M., Nilsson, K., Lukk, E., Vimberg, V., Tenson, T., and Ehrenberg, M. (2009). Erythromycin resistance by L4/L22 mutations and resistance masking by drug efflux pump deficiency. EMBO J. *28*, 736–744.

Malbruny, B., Canu, A., Bozdogan, B., Fantin, B., Zarrouk, V., Dutka-Malen, S., Feger, C., and Leclercq, R. (2002a). Resistance to quinupristin-dalfopristin due to mutation of L22 ribosomal protein in *Staphylococcus aureus*. Antimicrob. Agents Chemother. *46*, 2200–2207.

Malbruny, B., Nagai, K., Coquemont, M., Bozdogan, B., Andrasevic, A.T., Hupkova, H., Leclercq, R., and Appelbaum, P.C. (2002b). Resistance to macrolides in clinical isolates of *Streptococcus pyogenes* due to ribosomal mutations. J. Antimicrob. Chemother. *49*, 935–939.

McGuire, J.M., Bunch, R.L., Anderson, R.C., Boaz, H.E., Flynn, E.H., Powell, H.M., and Smith, J.W. (1952). Ilotycin, a new antibiotic. Schweiz. Med. Wochenschr. *82*, 1064–1065.

McLellan, T.J., Marr, E.S., Wondrack, L.M., Subashi, T.A., Aeed, P.A., Han, S., Xu, Z., Wang, I.K., and Maguire, B.A. (2009). A systematic study of 50S ribosomal subunit purification enabling robust crystallization. Acta Crystallogr. D Biol. Crystallogr. *65*, 1270–1282.

Meier, A., Kirschner, P., Springer, B., Steingrube, V.A., Brown, B.A., Wallace, R.J., Jr., and Bottger, E.C. (1994). Identification of mutations in 23S rRNA gene of clarithromycin-resistant *Mycobacterium intracellulare*. Antimicrob. Agents Chemother. *38*, 381–384.

Moore, S.D., and Sauer, R.T. (2008). Revisiting the mechanism of macrolide-antibiotic resistance mediated by ribosomal protein L22. Proc. Natl. Acad. Sci. USA *105*, 18261–18266.

Nakatogawa, H., and Ito, K. (2002). The ribosomal exit tunnel functions as a discriminating gate. Cell *108*, 629–636.

Otaka, T., and Kaji, A. (1975). Release of (oligo) peptidyl-tRNA from ribosomes by erythromycin A. Proc. Natl. Acad. Sci. USA *72*, 2649–2652.

Otwinowski, Z., and Minor, W. (1997). Processing of X-ray diffraction data collected in oscillation mode. Method Enzymol. *276*, 307–326.

Pardo, D., and Rosset, R. (1977). Properties of ribosomes from erythromycin resistant mutants of *Escherichia coli*. Mol. Gen. Genet. *156*, 267–271.

Pfister, P., Jenni, S., Poehlsgaard, J., Thomas, A., Douthwaite, S., Ban, N., and Bottger, E.C. (2004). The structural basis of macrolide-ribosome binding assessed using mutagenesis of 23S rRNA positions 2058 and 2059. J. Mol. Biol. *342*, 1569–1581.

Pihlajamaki, M., Jalava, J., Huovinen, P., and Kotilainen, P. (2003). Antimicrobial resistance of invasive pneumococci in Finland in 1999–2000. Antimicrob. Agents Chemother. *47*, 1832–1835.

Ramu, H., Vazquez-Laslop, N., Klepacki, D., Dai, Q., Piccirilli, J., Micura, R., and Mankin, A.S. (2011). Nascent peptide in the ribosome exit tunnel affects functional properties of the A-site of the peptidyl transferase center. Mol. Cell *41*, 321–330.

Schlunzen, F., Zarivach, R., Harms, J., Bashan, A., Tocilj, A., Albrecht, R., Yonath, A., and Franceschi, F. (2001). Structural basis for the interaction of antibiotics with the peptidyl transferase centre in eubacteria. Nature *413*, 814–821.

Schmeing, T.M., Huang, K.S., Strobel, S.A., and Steitz, T.A. (2005). An induced-fit mechanism to promote peptide bond formation and exclude hydrolysis of peptidyl-tRNA. Nature *438*, 520–524.

Schuttelkopf, A.W., and van Aalten, D.M.F. (2004). PRODRG: a tool for high-throughput crystallography of protein-ligand complexes. Acta Crystallogr. D *60*, 1355–1363.

Seidelt, B., Innis, C.A., Wilson, D.N., Gartmann, M., Armache, J.P., Villa, E., Trabuco, L.G., Becker, T., Mielke, T., Schulten, K., et al. (2009). Structural insight into nascent polypeptide chain-mediated translational stalling. Science *326*, 1412–1415.

Skinner, R., Cundliffe, E., and Schmidt, F.J. (1983). Site of action of a ribosomal RNA methylase responsible for resistance to erythromycin and other antibiotics. J. Biol. Chem. *258*, 12702–12706.

Sohmen, D., Chiba, S., Shimokawa-Chiba, N., Innis, C.A., Berninghausen, O., Beckmann, R., Ito, K., and Wilson, D.N. (2015). Structure of the *Bacillus subtilis* 70S ribosome reveals the basis for species-specific stalling. Nat. Commun. *6*, 6941.

Sothiselvam, S., Liu, B., Han, W., Ramu, H., Klepacki, D., Atkinson, G.C., Brauer, A., Remm, M., Tenson, T., Schulten, K., et al. (2014). Macrolide antibiotics allosterically predispose the ribosome for translation arrest. Proc. Natl. Acad. Sci. USA *111*, 9804–9809.

Sothiselvam, S., Neuner, S., Rigger, L., Klepacki, D., Micura, R., Vazquez-Laslop, N., and Mankin, A.S. (2016). Binding of macrolide antibiotics leads to ribosomal selection against specific substrates based on their charge and size. Cell Rep. *16*, 1789–1799.

Thompson, J.D., Gibson, T.J., and Higgins, D.G. (2002). Multiple sequence alignment using ClustalW and ClustalX. Curr. Protoc. Bioinformatics *Chapter 2*. Unit 2.3.

Tu, D., Blaha, G., Moore, P.B., and Steitz, T.A. (2005). Structures of MLSBK antibiotics bound to mutated large ribosomal subunits provide a structural explanation for resistance. Cell *121*, 257–270.

Vazquez-Laslop, N., Thum, C., and Mankin, A.S. (2008). Molecular mechanism of drug-dependent ribosome stalling. Mol. Cell *30*, 190–202.

Vazquez-Laslop, N., Ramu, H., Klepacki, D., Kannan, K., and Mankin, A.S. (2010). The key function of a conserved and modified rRNA residue in the ribosomal response to the nascent peptide. EMBO J. *29*, 3108–3117.

Vazquez-Laslop, N., Klepacki, D., Mulhearn, D.C., Ramu, H., Krasnykh, O., Franzblau, S., and Mankin, A.S. (2011). Role of antibiotic ligand in nascent peptide-dependent ribosome stalling. Proc. Natl. Acad. Sci. USA *108*, 10496–10501.

Voorhees, R.M., Weixlbaumer, A., Loakes, D., Kelley, A.C., and Ramakrishnan, V. (2009). Insights into substrate stabilization from snapshots of the peptidyl transferase center of the intact 70S ribosome. Nat. Struct. Mol. Biol. *16*, 528–533.

Wilson, D.N., Harms, J.M., Nierhaus, K.H., Schlunzen, F., and Fucini, P. (2005). Species-specific antibiotic-ribosome interactions: implications for drug development. Biol. Chem. *386*, 1239–1252.

Wilson, D.N., Arenz, S., and Beckmann, R. (2016). Translation regulation via nascent polypeptide-mediated ribosome stalling. Curr. Opin. Struct. Biol. *37*, 123–133.

Winn, M.D., Ballard, C.C., Cowtan, K.D., Dodson, E.J., Emsley, P., Evans, P.R., Keegan, R.M., Krissinel, E.B., Leslie, A.G.W., McCoy, A., et al. (2011). Overview of the CCP4 suite and current developments. Acta Crystallogr. D *67*, 235–242.

Wittmann, H.G., Stoffler, G., Apirion, D., Rosen, L., Tanaka, K., Tamaki, M., Takata, R., Dekio, S., and Otaka, E. (1973). Biochemical and genetic studies on two different types of erythromycin resistant mutants of *Escherichia coli* with altered ribosomal proteins. Mol. Gen. Genet. *127*, 175–189.

Woolhead, C.A., Johnson, A.E., and Bernstein, H.D. (2006). Translation arrest requires two-way communication between a nascent polypeptide and the ribosome. Mol. Cell *22*, 587–598.

Zaman, S., Fitzpatrick, M., Lindahl, L., and Zengel, J. (2007). Novel mutations in ribosomal proteins L4 and L22 that confer erythromycin resistance in *Escherichia coli*. Mol. Microbiol. *66*, 1039–1050.

Zhang, J., Pan, X.J., Yan, K.G., Sun, S., Gao, N., and Sui, S.F. (2015). Mechanisms of ribosome stalling by SecM at multiple elongation steps. Elife *4*, http://dx.doi.org/10.7554/eLife.09684.

STAR★METHODS

KEY RESOURCES TABLE

REAGENT or RESOURCE	SOURCE	IDENTIFIER
Bacterial Strains		
Deinococcus radiodurans R1	ATCC	ATCC #13939
Staphylococcus aureus Newman	NCTC	NCTC #8178
Chemicals, Peptides, and Recombinant Proteins		
Erythromycin	Sigma-Aldrich	Cat #E6376
[N-methyl-^{14}C]-Erythromycin	ARC	Cat #ARC-0467
Ammonium Chloride Crystal	Avantor	Cat #3384-12
Magnesium Chloride Hexahydrate	Avantor	Cat #0162-0250
Hepes	Fisher Scientific	Cat #BP310-1
2-Methyl-2,4-pentadiol	Acros	Cat #150340010
2-Ethyl-1,3-hexadiol	Merck	Cat #820032
Deposited Data		
Crystal structure of D50S-Ins3	This article	PDB: 4U67
Crystal structure of D50S-Ins3Ery	This article	PDB: 4WFN
Genome sequence of Dr-Ins3 and Sa-Δ2	This article	SRA: SRP107141
Software and Algorithms		
HKL2000	(Otwinowski and Minor, 1997)	http://www.hkl-xray.com/
CCP4	(Winn et al., 2011)	http://www.ccp4.ac.uk/
PHENIX	(Adams et al., 2010)	https://www.phenix-online.org/
COOT	(Emsley et al., 2010)	https://www2.mrc-lmb.cam.ac.uk/personal/pemsley/coot/
PyMOL	(DeLano, 2002)	https://www.pymol.org/

CONTACT FOR REAGENT AND RESOURCE SHARING

Further information and requests for resources and reagents should be directed to and will be fulfilled by the Lead Contact, Ada Yonath (ada.yonath@weizmann.ac.il) and Itai Wekselman (itai.wekselman@weizmann.ac.il).

EXPERIMENTAL MODEL AND SUBJECT DETAILS

Isolation of the Erythromycin Resistant Mutants

Dr-Ins3: Wild type *D. radiodurans* strain R1 (*Dra* R1) was obtained from the American Type Culture Collection (#13939). The MIC of Ery preventing growth of *Dra* R1 was determined to be 1.2 μg/ml on TGY plates. Resistant mutants were selected by spreading approximately 10^9 cells from overnight cultures onto TGY plates with 1.5 μg/ml Ery; each culture had originated from an individual colony grown on TGY (no antibiotic) to ensure that a mutant isolated on a given plate arose from a mutational event independent of events generating mutant colonies on other plates. After incubation at 30°C for 3-5 days, each plate usually had one or more visible colonies; only 1 colony per plate was selected for further analysis. The determined MIC of Ery for the Dr-Ins3 mutant is 10 μg/ml.

Sa-Δ2: The wild type *S. aureus* strain Newman was obtained from the National Collection of Type Cultures (NCTC 8178). The MIC of Ery for this strain was determined to be 0.5 μg/ml in cation-adjusted Mueller-Hinton broth. Wild type *S. aureus* was grown on tryptone soya agar (TSA) overnight at 37°C and individual colonies were streaked on TSA gradient plates containing 0 – 1 μg/ml Ery to select for mutants. Ery resistant mutants were continuously streaked on gradient plates with increasing Ery concentrations. The determined MIC of Ery for the Sa-Δ2 mutant is 8 μg/ml.

The genomes of the Dr-Ins3 and Sa-Δ2 mutants were sequenced. The analysis of the sequence revealed that both mutants contained alterations in the rplV gene encoding ribosomal protein uL22: An insertion of three residues (Val, Pro and Arg) after Arg88 in Dr-Ins3 and a deletion of two residues (Arg88 and Ala89) in Sa-Δ2. In both mutants, no additional mutations were identified in genes that are associated with resistance to Ery.

METHOD DETAILS

Bacterial Growth

The Dr-Ins3 strain was grown at 30°C in LB medium (pH=7.2) supplemented with 0.5 % glucose and 3 μg/ml of the antibiotic Ery. The growth began from a single colony that was transferred to a tube with 1.5 ml liquid medium and incubated for 24 h. 500 μl of the growing culture was transferred to a Falcon tube with 5 ml medium and incubated for additional 24 h. The culture was diluted 1:10 and incubated for 8 h in a 250 ml flask with 50 ml medium. The culture was diluted again (1:20) and incubated in a 2 l flask containing 500 ml medium for 24 h. The final growth stage was done in a 10 l fermenter under constant conditions of pH (7.2) and oxygen (80%). The culture was grown to a final OD_{600} of 3.

The Sa-Δ2 strain was cultured overnight at 37°C in tryptone soya broth (TSB) supplemented with 2 μg/ml Ery, inoculated from a single colony. From this culture, 2 l batches of the final culture were prepared in a fermenter under constant conditions of pH (7.3) with aeration, by inoculating 5 mL Sa-Δ2 culture per 1 l TSB supplemented with 2 μg/ml Ery. Cells were harvested in exponential phase ($OD_{600} \sim 0.7$). The bacterial cells were harvested by continuous-flow centrifugation. The bacterial paste was flash frozen in liquid nitrogen and stored at -80°C or used immediately for ribosome purification.

Purification of the Large Ribosomal Subunit

The purification of D50S-Ins3 was based on the protocol developed by Pfizer Inc (McLellan et al., 2009). The bacterial cells were suspended in $H_{10}M_{30}N_{150}\beta_6$ buffer (10 mM Hepes pH=7.8, 30 mM $MgCl_2$, 150 mM NH_4Cl, 6 mM β-mercaptoethanol) and DNase RNase free (Roche Diagnostics) was added (1 μl per 1 ml of buffer). The cells were broken by one passage through a French pressure cell at 10,000 PSI. The cell lysate was centrifuged for 45 min at 20,000 rpm in a Ti-70 rotor. The clear supernatant was collected and directly loaded onto a 10-40% linear sucrose gradient (in the $H_{10}M_{30}N_{150}\beta_6$ buffer) and centrifuged at 25,000 rpm for 16.5 h in a Ti-15 zonal rotor. The gradient was pumped out through an UV detector (260 nm) and the fractions containing the 70S ribosomes were collected. The 70S fraction was concentrated by ultrafiltration using the Pelicon device (Millipore). The sample was loaded onto a second (10-40 %) linear sucrose gradient in $H_{10}M_1N_{100}\beta_6$ (10 mM Hepes pH=7.8, 1 mM $MgCl_2$, 100 mM NH_4Cl, 6 mM β-mercaptoethanol) and centrifuged at 27,000 rpm for 17.5 h in Ti-15 zonal rotor. The fractions containing the 50S subunits were collected and centrifuged at 40,000 rpm for 19 h in a Ti-70 rotor. The pellets were resuspended in the $H_{10}M_{15}N_{75}$ buffer (10 mM Hepes pH=7.8, 15 mM $MgCl_2$, 75 mM NH_4Cl). The samples were centrifuged again in a TLA100.2 rotor at 75,000 rpm for 1.5 h. The pellets were resuspended in the $H_{10}M_{15}N_{75}$ buffer to a final concentration of 800-1000 A_{260} ml^{-1}. The samples were flash-frozen in liquid nitrogen for storage at -80°C.

For the Sa-Δ2 ribosome purification, the cells were lysed enzymatically by resuspension in the $H_{10}M_{30}N_{150}\beta_6$ buffer (10 mM Hepes pH=7.3, 30 mM $MgCl_2$, 150 mM NH_4Cl, 6 mM β-mercaptoethanol) supplemented with lysostaphin (50 μg/mL) and incubated for 45 min at 37 °C. The cell lysate was centrifuged for 45 min at 20,000 rpm in a Ti-70 rotor. The clear supernatant was layered on a 1.1 M sucrose cushion and centrifuged for 20 h at 40,000 rpm in a Ti-70 rotor. The pellet was dissolve in the $H_{10}M_{14}N_{100}K_{50}\beta_6$ buffer (10 mM Hepes pH=7.3, 14 mM $MgCl_2$, 100 mM NH_4Cl, 50 mM KCl, 6 mM β-mercaptoethanol). The sample was layered on a second 1.1 M sucrose cushion and centrifuged for 20 h at 40,000 rpm in a Ti-70 rotor. The sample was loaded onto a linear (10-40 %) sucrose gradient in the $H_{10}M_1N_{100}K_{50}$ buffer (10 mM Hepes pH=7.3, 1 mM $MgCl_2$, 100 mM NH_4Cl, 50 mM KCl) and centrifuged at 27,000 rpm for 17.5 h in a Ti-15 zonal rotor. The fractions containing the 30S and 50S subunits were collected and centrifuged at 40,000 rpm for 19 h in a Ti-70 rotor. The pellets were resuspended in the $H_{10}M_{10}N_{60}K_{15}$ buffer (10 mM Hepes pH=7.6, 10 mM $MgCl_2$, 60 mM NH_4Cl, 15 mM KCl. The samples were centrifuged again in a TLA100.2 rotor at 75,000 rpm for 1.5 h. The pellets were resuspended in the $H_{10}M_{10}N_{60}K_{15}$ buffer to a final concentration of 800-1000 A_{260} ml^{-1}. The samples were flash-cooled in liquid nitrogen for storage at -80 °C.

Erythromycin Binding

Ery binding assays were performed according to the filter binding method. 0.1μM of 50S subunits were incubated at 37°C for 15 min with different concentrations of [N-methyl-^{14}C]-Ery (American Radiolabeled Chemicals; 55 mCi $mmol^{-1}$; 100 μCi ml^{-1}) in Ery binding buffer (50 mM Tris-HCl pH 7.8; 16 mM Mg acetate; 60 mM KCl; 100 μl final volume). The assay mix was poured through a 0.45 μm nitrocellulose filter (Millipore). Filters were washed three times, each with 3 ml Ery wash buffer (25 mM Tris-HCl pH= 7.8, 20 mM Mg acetate, 60 mM KCl). The amount of radioactive Ery bound to the ribosomes was measured by liquid scintillation counting of the filters (Beckman-Coulter LS 6500). Assays were always carried out in triplicates. The analysis of the binding data was performed with Prism (v. 7.0, GraphPad Software Inc., San Diego, CA).

Crystallization

Crystallization conditions were based on those used for the crystallization of native D50S (Harms et al., 2001). The D50S-Ins3 subunits were heat activated (for 15-30 min) at 37°C before crystallization. The crystals were obtained at 20°C by the hanging-drop vapor diffusion technique. The co-crystallization of D50S-Ins3 with Ery was done in the presence of five-fold excess of Ery in the drop. After the crystals reached their maximal size (2-3 weeks), they were transferred to stabilizing solution: 30% 2-ethyl-1,3-hexandiol (EHD)-ethanol 1:2. Prior to the data collection the crystals were transferred for 10 min to cryo-protecting solution (15% EHD-ethanol 1:2, 15% 2-methy-2,4-pentanediol) and flash-cooled in liquid nitrogen. Crystals of the D50S-Ins3Ery complex were transferred to stabilizing and cryo-protecting solutions containing 0.05 mM Ery.

Data Collection and Processing

The X-ray diffraction data were collected at 100K at the ID23-2 microfocus beamline at the ESRF, Grenoble, France. The data were processed by HKL2000 (Otwinowski and Minor, 1997) and CCP4 (Winn et al., 2011).

Structure Solution, Model Building and Refinement

The structures were solved by molecular replacement using PHASER as implemented in PHENIX (Adams et al., 2010). The native D50S structure (PDB code: 2ZJR) omitting the uL22 loop (residues 100-125) was used as a search model. The initial solution was subjected to rigid-body refinement, followed by several cycles of positional and grouped B-factor refinement using PHENIX. The tracing of the uL22 loop and changes in the coordinates of rRNA nucleotides dictated by the difference electron density maps were performed using COOT (Emsley et al., 2010). The initial model for the antibiotic Ery was derived from the crystal structure of the *T. thermophilus* 70S ribosome in complex with Ery (PDB code: 4V7X, Bulkley et al., 2010) and the chemical restraints for the antibiotic were prepared by the PRODRG server (Schuttelkopf and van Aalten, 2004). The coordinates of the antibiotic were fitted in COOT to the sigma-weighted difference electron density maps, followed by cycles of positional and grouped B-factor refinement using PHENIX.

Figure Generation and Sequence Alignment

All figures were generated with PyMOL (DeLano, 2002). L22 multiple sequence alignment was performed by ClustalW (Thompson et al., 2002) and presented by Jalview (Clamp et al., 2004).

QUANTIFICATION AND STATISTICAL ANALYSIS

The binding data of radiolabeled Ery were fitted to a one-site specific binding model to determine the K_D in Prism (v. 7.0, GraphPad Software Inc., San Diego, CA).

DATA AND SOFTWARE AVAILABILITY

Atomic coordinates and structure factors for the D50S-Ins3 and D50S-Ins3Ery have been deposited in the Protein Data Bank (PDB) under accession codes 4U67 and 4WFN, respectively. The raw genomic sequencing data of the Dr-Ins3 and Sa-Δ2 mutants have been deposited in the National Center for Biotechnology Information (NCBI) Sequence Read Archive (SRA) (http://www.ncbi.nlm.nih.gov/sra/) under accession number SRP107141.